2018 European Control Conference (ECC)
June 12-15, 2018. Limassol, Cyprus

Film growth minimization in a Li-ion cell: a Pseudo Two Dimensional model-based optimal charging approach

Andrea Pozzi, Marcello Torchio, Davide M. Raimondo

Abstract— **Safety, fast charging and aging are among the most important issues when dealing with high power battery packs in electric and hybrid vehicles. Today's charging strategies are designed to guarantee safe operation in a conservative way, but are far from being optimal in terms of aging reduction and time charging minimization. For this reason, the interest of the research is focused on developing model-based battery management systems. Comparing standard charging strategies with health-aware optimization-based ones is difficult since they usually provide different charging times: are we willing to charge the battery in more time if this comes with an aging reduction? When a customer is faced with such a question, the answer is not so trivial. For this reason, in this paper we provide health-aware Pseudo Two Dimensional model-based strategies with the same charging time of standard CC-CV protocols. The results show that significant aging improvements can be obtained, even by constraining the charging time to be the same as the CC-CV protocol.**

I. Introduction

Nowadays the popular charging strategies implemented by Battery Management Systems (BMSs) still remain Constant Current - Constant Voltage (CC-CV), MultiStage Constant Current (MSCC), pulse current and pulse voltage protocols [1]. Among all the recharging methods for Li-ion batteries, the CC-CV is the most widely used, due to the simple implementation: the approach first applies the current I_{cc} in a galvanostatic charge (CC), untill the voltage threshold V_{cv} is reached. Then a potentiostatic charge (CV) is applied, while the current through the cell decreases exponentially, untill the current cutting threshold I_{cut} is reached. Although the CC-CV protocol provides reasonable performance, it is based on conservative voltage terminal limits in order to guarantee safe operation during the whole battery lifetime, without accounting for battery changes with aging degradation. For this reason, the research challenge is to improve battery performances by developing model-based Advanced Battery Management Systems (ABMSs). Model Predictive Control (MPC) is particularly suitable for this purpose due to its ability of dealing with nonlinear systems and constraints. Despite over the years considerable predictive control strategies have been proposed as ABMSs [2], [3], [4], only few of them have focused on aging reduction [5], [6], [7], [8], [9], [10]. However, all the proposed approaches obtain an aging reduction to the detriment of the charging duration. Indeed, with a less aggressive charging strategy, it is straightforward to obtain aging reduction.

This paper presents, for the first time to the knowledge of the authors, an optimization-based charging strategy that relies on the well known Pseudo Two Dimensional (P2D, [11]) model, constraining the charging time to be the same as the CC-CV protocol. This peculiarity allows a fair comparison in terms of aging reduction over a whole charging procedure. Furthermore, in order to guarantee safe operation, the possibility to use a constraint on the plating side reaction overpotential instead of the more conservative terminal voltage limits is considered. The results emphasize the significant aging effects reduction for the same charging time, especially in terms of SEI layer thickness growing, for both the case of a constraint on the voltage and on the lithium plating.

The paper is organized as follows. In Sec. II a detailed first principles P2D model of the battery is presented as model for the control, focusing on the space discretization method (Sec. II-A). In Sec. III the health-optimal charging problem with fixed time is presented. In Sec. IV the results are shown, focusing on the improvements on battery performance provided by the optimization-based strategies compared to the standard CC-CV one. In Sec. V the presented work is summarized and possible future research is presented.

II. Electrochemical model of a Li-ion battery

In this section, the first principles Pseudo Two Dimensional model is presented in order to describe the electrochemical behavior of a Lithium ion cell. The model consists of nonlinear and tightly coupled partial differential algebraic equations (PDAEs), which are used to represent the conservation of mass and charge within the main sections of the Li-ion cell. In order to consider the presence of Solid-Electrolyte Interface (SEI) layer and to account for aging dynamics, the P2D equations are augmented as in [7].

With the term battery, it is common to refer to a series or parallel interconnection of cells. A Lithium ion cell is composed by five main sections: the positive current collector (a), the cathode (p), the separator (s), the anode (n) and the negative current collector (z). In the following, the index $i \in \{a, p, s, n, z\}$ is used to refer to the different sections of the battery, whose thickness is expressed with l_i. The structure anode-separator-cathode is immersed within an electrolyte solution, thus enabling ionic conduction. When carrying out a charging process, the Li-ions will *deintercalate* from the cathode and, flowing through the porous separator, will *intercalate* into the anode. The opposite process occurs

A. Pozzi and D.M. Raimondo are with the Dipartimento di Ingegneria Industriale e dell'Informazione, University of Pavia, 27100 Pavia, Italy. (e-mail:{andrea.pozzi03, davide.raimondo}@unipv.it)
M. Torchio is with the Dipartimento di Ingegneria Civile e Architettura, University of Pavia, 27100 Pavia, Italy. (e-mail: marcello.torchio01@ateneopv.it)

when a cell is discharged. The anodic bulk State of Charge (SOC) is defined as

$$\text{SOC}(t) := \frac{1}{l_n\, c_s^{\text{max,n}}} \int_0^{l_n} c_s^{\text{avg}}(x,t)\, dx. \tag{1}$$

where $t \in \mathbb{R}^+$ represents the time, $x \in \mathbb{R}$ is the one dimensional spatial variable, $c_s^{\text{max,n}}$ is the maximum concentration of Li-ions in the negative electrode and $c_s^{\text{avg}}(x,t)$ is the average concentration of solid particles, used to model, by the following polynomial approximation, the ionic diffusion occurring into (or out from) the porous matrix of the electrodes, during intercalation or deintercalation processes

$$\begin{aligned} \frac{\partial}{\partial t} c_s^{\text{avg}}(x,t) &= -\frac{3}{R_s} j_{\text{int}}(x,t) \\ c_s^*(x,t) - c_s^{\text{avg}}(x,t) &= -\frac{R_s}{5 D_{\text{eff}}^s} j_{\text{int}}(x,t), \end{aligned} \tag{2}$$

where $c_s^*(x,t)$ is the surface concentration of solid particles, R_s and D_{eff}^s account for the particle radius and effective diffusion coefficients of the solid phases and the function $j_{\text{int}}(x,t)$ represents the intercalation/deintercalation part of the ionic flux $j(x,t)$, which is given by

$$j(x,t) = j_{\text{int}}(x,t) + j_{\text{side}}(x,t),$$

where $j_{\text{side}}(x,t)$ accounts for the electrolyte-anode interface side reactions that occur during charging phases, while the plating side reaction flux is assumed to be negligible. The flow of ions, that occurs during operating conditions inside the electrolyte solution, is modeled using a diffusion equation

$$\epsilon \frac{\partial}{\partial t} c_e(x,t) = \frac{\partial}{\partial x}\left[D_{\text{eff}} \frac{\partial c_e(x,t)}{\partial x} \right] + a(1-t_+) j(x,t),$$

where $c_e(x,t)$ is the electrolytic ion concentration, t_+ defines the transference number, a is the particle surface area to volume ratio, D_{eff} accounts for the effective diffusion coefficients in the electrolyte (according to Bruggeman's theory), ϵ represents the material porosity. The intercalation part of the ionic flux is governed by the Butler-Volmer equations

$$j_{\text{int}}(x,t) = 2\frac{i_{0,\text{int}}}{F} \sinh\left[\frac{0.5F}{\text{R}T(x,t)} \eta_{\text{int}}(x,t) \right],$$

where $\eta_{\text{int}}(x,t)$ represents the electrodes overpotential, $T(x,t)$ is the cell temperature, while F and R are the Faraday's constant and the universal gas constant, respectively. The exchange current density $i_{0,\text{int}}$ is defined as

$$i_{0,\text{int}} = F k_{\text{eff}} \sqrt{c_e(x,t)(c_s^{\text{max}} - c_s^*(x,t)) c_s^*(x,t)},$$

where c_s^{max} is the maximum allowed concentration in each electrode and k_{eff} the effective kinetic reaction rate. A Tafel relation is used to model the term $j_{\text{side}}(x,t)$ as follows [12]

$$j_{\text{side}}(x,t) = -\frac{i_{0,\text{side}}(t)}{F} \exp\left(\frac{0.5F}{\text{R}T(x,t)} \eta_{\text{side}}(x,t) \right), \tag{3}$$

where $i_{0,\text{side}}(t)$ and $\eta_{\text{side}}(x,t)$ are respectively the side reaction exchange current density and overpotential. According to the authors in [6], is shown that the side reaction exchange current $i_{0,\text{side}}(t)$ is strictly influenced by the applied current density $I_{\text{app}}(t)$. Due to the impossibily of measuring such quantities, no experimental data are available relating these two indexesa. For this reason the following empirical equation is used to model their relation [13]

$$i_{0,\text{side}}(t) = i_{0,\text{base}} \left(\frac{I_{\text{app}}(t)}{I_{1C}} \right)^{\omega} \tag{4}$$

The SEI layer contributes to the cell aging process, growing with the number of cycles. In order to account for its evolution, the following equation is considered [12]

$$\frac{\partial}{\partial t}\delta(x,t) = -\frac{M_w}{\rho} j_{\text{side}}(x,t), \tag{5}$$

where M_w is the molar weight of the electrode and $\delta(x,t)$ represents the film thickness. However, the formation of the SEI layer starts right after a cell manufacturing. Therefore the overall film resistance is given by the sum of two contributes

$$R_f(t) = R_{\text{SEI}} + \frac{\bar{\delta}(t)}{\nu},$$

where R_{SEI} is the initial SEI layer resistance, ν is the film admittance, while $\bar{\delta}(t)$ is the film thickness spatial mean

$$\bar{\delta}(t) := \frac{1}{l_n} \int_0^{l_n} \delta(x,t)\, dx. \tag{6}$$

It is important to underline that during the *intercalation* and *deintercalation* processes, the Li-ions diffuse within the solid particles of the porous electrodes as a function of $j_{\text{int}}(x,t)$, while the $j_{\text{side}}(x,t)$ plays a role at the anode side for accounting for the presence of the SEI layer. According to the Ohm's law, the solid phase potential $\Phi_s(x,t)$ inside the two electrodes is modeled as follows

$$\frac{\partial}{\partial x}\left[\sigma_{\text{eff}} \frac{\partial}{\partial x} \Phi_s(x,t) \right] = aFj(x,t),$$

where σ_{eff} is the electrodes effective conductivity. The cell terminal voltage is

$$V_{\text{out}}(t) := \Phi_s(0,t) - \Phi_s(L,t), \tag{7}$$

where $L = \sum_i l_i$ is the overall battery thickness. A modified Ohm's law is used to represent the charge conservation within the electrolyte

$$\begin{aligned} aFj(x,t) + \frac{\partial}{\partial x}\left[\kappa_{\text{eff}} \frac{\partial}{\partial x} \Phi_e(x,t) \right] = \\ \frac{\partial}{\partial x}\left[\frac{2\kappa_{\text{eff}} \text{R}T(x,t)}{F}(1-t_+) \frac{\partial}{\partial x} \ln c_e(x,t) \right], \end{aligned}$$

where $\Phi_e(x,t)$ is the electrolytic potential and κ_{eff} is the effective conductivity of the liquid phase. The temperature dynamics are modeled by an energy balance,

$$\rho C_p \frac{\partial}{\partial t} T(x,t) = \frac{\partial}{\partial x}\left[\lambda \frac{\partial}{\partial x} T(x,t) \right] + Q_{\text{source}}(x,t) \tag{8}$$

where C_p is the material specific heat, λ is the heat diffusion coefficient, ρ represents the density,

$$Q_{\text{source}}(x,t) = Q_{\text{ohm}}(x,t) + Q_{\text{rev}}(x,t) + Q_{\text{rxn}}(x,t),$$

and the terms $Q_{\text{ohm}}(x,t)$, $Q_{\text{rev}}(x,t)$, and $Q_{\text{rxn}}(x,t)$ are the ohmic, reversible, and reaction heat sources terms [14]. The above set of nonlinear and tightly coupled partial differential and algebraic equations are used to describe the P2D model. A thorough description of such model, its parameters and boundary conditions can be found in [15], [7], [12].

A. Numerical implementation of P2D model

The independent space variable x in the set of PDAEs above has been spatially discretized according to the Finite Volume Method (FVM), and the model results into a set of Differential Algebraic Equations (DAEs)

$$\begin{cases} \dot{x}(t) = f\left(x(t), z(t), u(t)\right) \\ z(t) = h\left(x(t), z(t), u(t)\right) \\ y(t) = \left[x(t)^T \; z(t)^T\right]^T \end{cases} \tag{9}$$

where $x(t) \in \mathbb{R}^{n_d}$ and $z(t) \in \mathbb{R}^{n_a}$ are respectively the differential and algebraic state vectors, $y(t) \in \mathbb{R}^{n_d+n_a}$ are the system outputs and $u(t) \in \mathbb{R}$ is the current density input, n_d and n_a are respectively the number of differential and algebraic states. In particular

$$\begin{aligned} x(t) &= \left[x_{c_e}(t) \; x_{c_s^{\text{avg}}}(t) \; x_T(t) \; x_\delta(t)\right]^T \\ z(t) &= \left[z_{j_{\text{int}}}(t) \; z_{\Phi_s}(t) \; z_{\Phi_e}(t) \; z_{j_{\text{side}}}(t)\right]^T \end{aligned} \tag{10}$$

where each component of the state vectors in (10) is a vector given by the value of that component in the different finite volumes. As shown in Fig. 1, the positive current collector has been discretized into N_a spatial points, the positive electrode into N_p, the separator into N_s, the negative electrode into N_n and the negative current collector into N_z. In particular one has for the differential states

$$\begin{aligned} x_{c_e} &= [c_{e,\{p,1\}}, ..., c_{e,\{p,N_p\}}, c_{e,\{s,1\}}, ..., c_{e,\{s,N_s\}}, \\ &\quad c_{e,\{n,1\}}, ..., c_{e,\{n,N_n\}}] \\ x_{c_s^{\text{avg}}} &= [c^{\text{avg}}_{s,\{p,1\}}, ..., c^{\text{avg}}_{s,\{p,N_p\}}, c^{\text{avg}}_{s,\{n,1\}}, ..., c^{\text{avg}}_{s,\{n,N_n\}}] \\ x_T &= [T_{\{a,1\}}, ..., T_{\{a,N_a\}}, T_{\{p,1\}}, ..., T_{\{p,N_p\}}, \\ &\quad T_{\{s,1\}}, ..., T_{\{s,N_s\}}, T_{\{n,1\}}, ..., T_{\{n,N_n\}}, \\ &\quad T_{\{z,1\}}, ..., T_{\{z,N_z\}}] \\ x_\delta &= [\delta_{\{n,1\}}, ..., \delta_{\{n,N_n\}}] \end{aligned}$$

and for the algebraic states

$$\begin{aligned} z_{j_{\text{int}}} &= [j_{\text{int},\{p,1\}}, ..., j_{\text{int},\{p,N_p\}}, j_{\text{int},\{n,1\}}, ..., j_{\text{int},\{n,N_n\}}] \\ z_{\Phi_s} &= [\Phi_{s,\{p,1\}}, ..., \Phi_{s,\{p,N_p\}}, \Phi_{s,\{n,1\}}, ..., \Phi_{s,\{n,N_n\}}] \\ z_{\Phi_e} &= [\Phi_{e,\{p,1\}}, ..., \Phi_{e,\{p,N_p\}}, \Phi_{e,\{s,1\}}, ..., \Phi_{e,\{s,N_s\}}, \\ &\quad \Phi_{e,\{n,1\}}, ..., \Phi_{e,\{n,N_n\}}] \\ z_{j_{\text{side}}} &= [j_{\text{side},\{n,1\}}, ..., j_{\text{side},\{n,N_n\}}] \end{aligned}$$

The expression of the terminal voltage in (7) becomes

$$V_{\text{out}}(t) = \Phi_{s,\{p,1\}}(t) - \Phi_{s,\{n,N_n\}}(t)$$

while the spatial integral becomes a summation of discretized quantities for (1) and (6)

$$\text{SOC}(t) = \frac{100}{N_n c_s^{\text{max,n}}} \sum_{j=1}^{N_n} c^{\text{avg}}_{s,\{n,j\}}(t)$$

$$\bar{\delta}(t) := \frac{1}{N_n} \sum_{j=1}^{j=N_n} \delta_{\{n,j\}}(t)$$

The spatial mean of the temperature is defined as follows

$$\overline{T}(t) := \frac{1}{N_{tot}} \sum_{i \in \{a,p,s,n,z\}} \sum_{j=1}^{N_i} T_{\{i,j\}}(t)$$

where $N_{\text{tot}} = N_a + N_p + N_s + N_n + N_z$. Furthermore in this work all the states are assumed to be measurable at each sampling time, as specified by the output equation in (9). This assumption simplifies a lot the optimization problem, since the design of a suitable observer is not considered. However this field has raised the interest of many authors that propose different solutions (extended kalman filtering [16], [17], sliding-mode observers [18], [19]), and might be object of future work.

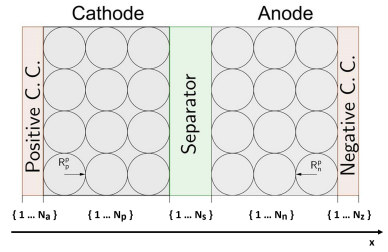

Fig. 1: Scheme of the space discretization method.

III. Optimization problem

The model described in Sec. II-A is used to compute an health-aware charging strategy that is optimal compared with the standard CC-CV protocol. Therefore the space discretized set of differential algebraic equations is then discretized in time using the direct collocation method [20]. In order to make the comparison fair we will constrain the optimization-based strategy charging time to the one of the reference standard protocol (t_{ref}). First a simulation of standard CC-CV charging procedure is performed with LIONSIMBA [15], a Matlab framework that numerically implements the P2D model equations, and the simulated states evolution is used as initial guess for the optimization. Aging dynamics are taken into account by setting the *EnableAgeing* parameter of the model equal to one, during the parameters declaration. The optimal control input is the solution of a

nonlinear optimal control problem, mathematically formulated as follows

$$\underset{u(\cdot)}{\text{minimize}} \quad \int_{t_0}^{t_0+t_{\text{ref}}} l(x(\tau),u(\tau))\,d\tau + m(x(t_0+t_{ref})) \tag{11a}$$

$$\text{subject to} \quad \overline{T}(t) \leq T_{\max}, \tag{11b}$$

$$V_{\min} \leq V_{\text{out}(t)} \leq V_{\max}, \tag{11c}$$

$$\text{SOC}_{\min} \leq \text{SOC}(t) \leq \text{SOC}_{\max}, \tag{11d}$$

$$I_{\min} \leq u(t) \leq I_{\max}, \tag{11e}$$

$$\text{SOC}(t_0+t_{\text{ref}}) = \text{SOC}_{\text{ref}}, \tag{11f}$$

$$\text{model dynamics in Sec. (9).} \tag{11g}$$

where t_0 is the starting time, t_{ref} is the standard protocol charging time to reach a state of charge SOC_{ref}. The objective function is composed by a nonlinear quadratic *Lagrange* term in order to regularize the solution and to improve solver efficiency

$$l(x(t),u(t)) = q(\text{SOC}(t)-\text{SOC}_{\text{ref}})^2 + ru^2(t)$$

and a *Mayer* term so as to penalize the film thickness at the end of the charge

$$m(x(t_0+t_{\text{ref}})) = \gamma\bar{\delta}(t_0+t_{ref})$$

where $q \geq 0$, $r > 0$ and $\gamma > 0$ are suitable weighting factors that adjust the trade-off between fast charging and aging processes. In the following we will set $q = r = 10^{-4}$ and $\gamma = 1$. The optimal control problem in (11) defines as control task the minimization of aging effects while battery charging procedure, subject to thermal constraints (11b), voltage constraints (11c), SOC constraints (11d), and limited input current (11e), in order to guarantee safe operation. The reaching of the reference SOC in the desired fixed time is imposed by (11f). Although the optimization relies on a continuous time model, the practical implementation of the strategy requires the use of piece-wise constant inputs. Taking into account the trade-off between accuracy and computational cost, a step size of $t_s = 100s$ has been chosen. Equations in (11) lead to a large-scale sparse nonlinear programming problem which is solved by IPOPT [21], using the solver *ma27*. Due to the nonlinear problem formulation, only a local minimum can be achieved. The exact derivatives are computed using CasADi [22], a symbolic framework for automatic differentiation, that is essential for the efficient solution of the problem. Furthermore, a scaling of all the variables is performed in order to improve significantly solver efficiency. After the computation of the optimal control inputs, the battery charging procedure is simulated with LIONSIMBA, so to evaluate the effectiveness of the proposed strategies on a realistic simulator.

Before presenting the obtained results, in the next section the replacement of (11c) with a different constraint that guarantees the same safety performances of the cell battery [5] is considered.

A. Suitable constraint in order to avoid plating deposition

The constraint on the terminal voltage is a way to avoid regimes in which undesirable side reactions become significant [23], [24]. Among them the most important is the lithium plating deposition, a cathodic side reaction taking place in the negative electrode when the correspondent overpotential becomes negative [25]. Despite the terminal limits are chosen to be conservative, standard charging operations with aging batteries might be dangerous anyway, due to the change over time of physical parameters. For this reason, it is of interest to directly constrain the plating side reaction overpotential to be positive. The overpotential can be approximated as

$$\eta_{\text{pl}}(x,t) = \Phi_s(x,t) - \Phi_e(x,t)$$

where the side reaction equilibrium potential is null and the plating side reaction flux is supposed to be negligible. Its space discretization is given by

$$z_{\eta_{\text{pl}}} = [\eta_{\text{pl},\{p,1\}},...,\eta_{\text{pl},\{p,N_p\}},\eta_{\text{pl},\{n,1\}},...,\eta_{\text{pl},\{n,N_n\}}]$$

A suitable constraint able to replace (11c), in order to avoid lithium plating deposition during the whole battery life, is

$$\eta_{\text{pl},\{i,j\}} > 0, \qquad i \in \{p,n\}, \qquad j = 1...n_i \tag{12}$$

In Sec. IV-A the solution of the optimization problem in (11) is compared with the CC-CV protocol. Furthermore, in Sec. IV-B a second optimization-based charging protocol is obtained by substituting the (11c) with (12).

IV. Results

In this section, a comparison between the two different optimization-based charging strategies and a standard CC-CV protocol is shown. For all the simulations, the battery cell is in a rest initial condition with $\text{SOC}(t_0) = 10\%$, and $\text{SOC}_{\text{ref}} = 74\%$ is reached in a fixed charging time of $t_{\text{ref}} = 3000s$. The standard CC-CV charging protocol presents $I_{\text{cc}} = 35\frac{A}{m^2}$, $V_{\text{cv}} = 4.07\,V$ and $I_{\text{cut}} = 5\frac{A}{m^2}$. For all the optimization-based strategies the applied current density has been bounded within $I_{\min} = 0$ and $I_{\max} = 2C$, with $C = 29.3\frac{A}{m^2}$. Different simulation settings provide analogs results. The main features of the different simulations are summarized in Table I, where $V_{\text{out}}^{\max}$ is the maximum voltage reached, $T^{\max}$ the maximum temperature, $\eta_{\text{pl}}^{\min}$ the minimum plating side reaction overpotential, $u^{\max}$ the maximum input current and $\bar{\delta}_{\%}$ the film thickness reduction in percentage. All the results are shown in Fig. 2.

	CC-CV	Optimal$_V$	Optimal$_{pl}$
$V_{\text{out}}^{\max}$ $[V]$	4.07	4.07	4.12
$T^{\max}$ $[K]$	305.35	304.77	302.41
$\eta_{\text{pl}}^{\min}$ $[V]$	0.0749	0.0793	0.0734
$u^{\max}$ $[A]$	35.00	56.33	47.60
$\bar{\delta}_{\%}$ $[\%]$	-	-2.11%	-13.71%

TABLE I: Main features of different charging protocols.

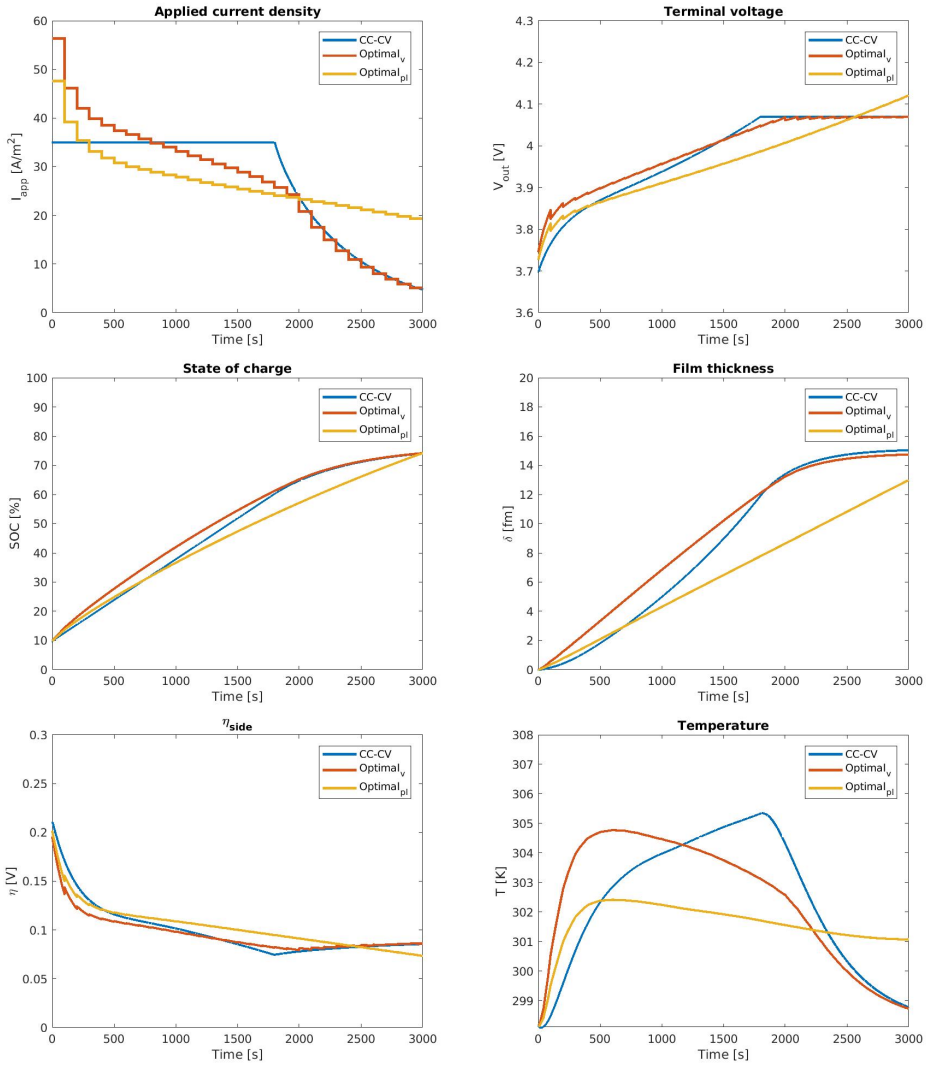

Fig. 2: Input and states evolution of the cell battery due to CC-CV protocol and optimization based strategies.

A. *Results with voltage constraint*

In the following, $V_{\min} = 2.5\,V$ and $V_{\max} = V_{\text{cv}}$ are considered as voltage terminal bounds. It can be noticed that the more significant variations introduced by the optimization-based strategy lie in the charging regimes in which the voltage constraint is not active (i.e. $t < 2000s$). For $t \geq 2000s$ the state evolution follows the CC-CV one. However, despite the higher value of input current applied, the optimization-based strategy leads to a 2.11% reduction of the spatial mean of film thickness at the end of the charging procedure, with a reduction of the maximum temperature of $0.58K$. Furthermore the maximum voltage and the minimum plating side reaction overpotential reached are the same of the CC-CV protocol, because of the voltage constraint.

B. *Results with plating constraint*

The solution of the optimization problem by substituting (11c) with (12) in its formulation, leads to a completely different states evolution than the CC-CV standard charging protocol, with benefits from every point of view in terms of aging:

1) the spatial mean of the film thickness at the end of the charging procedure is reduced of about 13.71%;
2) the maximum temperature is reduced of about $3K$;

Furthermore the raising of the voltage over the maximum value reach by the CC-CV protocol does not degrade battery performance since the plating side reaction overpotential is far away enough from critical value for lithium plating deposition, being positive during the whole charging procedure. One of the most important aspects emerging from the optimal solution with plating constraint is the linearity growth of film thickness, that seems to be the key point in its reduction. At the same time this can be seen in the side reaction flux profile (Fig. 3), that the optimization-based strategy try to keep as constant as possible, carrying out a sort of hysteresis control around a fixed value. Therefore better results can be obtained increasing the control variables number, although this increases computational cost and the average time to

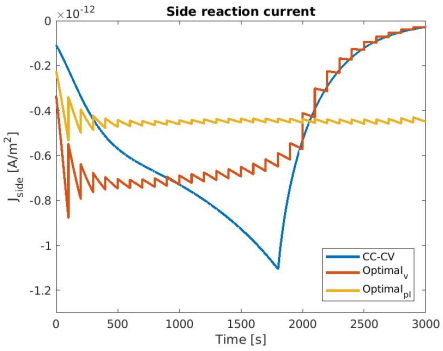

Fig. 3: Side reaction flux profiles.

get a feasible solution. Using $t_s = 100s$ the time needed to solve the problem with plating overpotential constraint is $5s$ in average. However with $t_s = 50s$ the time needed to solve the problem raises to $50s$ in average, that might be challenging for online closed-loop solution of the problem. The simulations are performed on a Ubuntu 17.04 machine with 4Gbytes of RAM and i5vPro processor 2.5 GHz.

V. Conclusions

To the best of our knowledge, all the existing health aware model based charging strategies follow a trivial approach to reduce aging, that is by increasing the charging time. In order to ease the user in the choice of an optimal charging procedure and make a comparison with standard charging protocols fair, in this paper the charging time has been kept equal to the CC-CV one, while a significant aging effects minimization is shown. For this reason the prediction horizon have to cover the whole charging procedure, increasing computational burden. Although automatic differentiation increase the efficiency of the problem solution, the implementation of an optimal state-feedback control law, using such a complex electrochemical model, still remain a critical aspect. Future work includes the design of a suitable observer for the electrochemical model, in order to relax the assumptions of measurable states, and experimental validation of the proposed optimization-based charging strategy.

References

[1] W. Shen, T. T. Vo, and A. Kapoor, "Charging algorithms of lithium-ion batteries: An overview," in *Industrial Electronics and Applications (ICIEA), 2012 7th IEEE Conference on*. IEEE, 2012, pp. 1567–1572.

[2] J. Yan, G. Xu, H. Qian, Y. Xu, and Z. Song, "Model predictive control-based fast charging for vehicular batteries," *Energies*, vol. 4, no. 8, pp. 1178–1196, 2011.

[3] M. Torchio, N. A. Wolff, D. M. Raimondo, L. Magni, U. Krewer, R. B. Gopaluni, J. A. Paulson, and R. D. Braatz, "Real-time Model Predictive Control for the Optimal Charging of a Lithium-ion Battery," in *Proceedings of the American Control Conference*, 2015, pp. 4536–4541.

[4] M. A. Xavier and M. S. Trimboli, "Lithium-ion battery cell-level control using constrained model predictive control and equivalent circuit models," *Journal of Power Sources*, vol. 285, pp. 374–384, 2015.

[5] R. Klein, N. A. Chaturvedi, J. Christensen, J. Ahmed, R. Findeisen, and A. Kojic, "Optimal charging strategies in lithium-ion battery," in *American Control Conference (ACC), 2011*. IEEE, 2011, pp. 382–387.

[6] S. J. Moura, J. C. Forman, S. Bashash, J. L. Stein, and H. K. Fathy, "Optimal control of film growth in lithium-ion battery packs via relay switches," *IEEE Transactions on Industrial Electronics*, vol. 58, no. 8, pp. 3555–3566, 2011.

[7] M. Torchio, L. Magni, R. D. Braatz, and D. M. Raimondo, "Optimal health-aware charging protocol for Lithium-ion batteries: A fast model predictive control approach," in *Proceedings of the 11th International Symposium on Dynamics and Control of Process Systems, including Biosystems*, 2016, pp. 827–832.

[8] M. Torchio, L. Magni, R. B. Gopaluni, R. D. Braatz, and D. M. Raimondo, "Optimal Charging of a Li-ion Cell:A Hybrid Model Predictive Control Approach," in *Proceedings of the Conference on Decision and Control*, 2016, p. accepted.

[9] M. Torchio, L. Magni, R. D. Braatz, and D. Raimondo, "Design of piecewise affine and linear time-varying model predictive control strategies for advanced battery management systems," *Journal of The Electrochemical Society*, vol. 164, no. 4, pp. A949–A959, 2017.

[10] S. Lucia, M. Torchio, D. M. Raimondo, R. Klein, R. D. Braatz, and R. Findeisen, "Towards adaptive health-aware charging of li-ion batteries: A real-time predictive control approach using first-principles models," in *American Control Conference (ACC), 2017*. IEEE, 2017, pp. 4717–4722.

[11] C. M. Doyle, "Design and simulation of lithium rechargeable batteries," *Lawrence Berkeley National Laboratory*, 2010.

[12] P. Ramadass, B. Haran, P. M. Gomadam, R. White, and B. N. Popov, "Development of First Principles Capacity Fade Model for Li-Ion Cells," *Journal of The Electrochemical Society*, vol. 151, no. 2, p. A196, 2004.

[13] M. Rashid and A. Gupta, "Mathematical model for combined effect of SEI formation and gas evolution in Li-ion batteries," *ECS Electrochemistry Letters*, vol. 3, no. 10, pp. A95–A98, 2014.

[14] K. Kumaresan, G. Sikha, and R. E. White, "Thermal model for a Li-ion cell," *Journal of The Electrochemical Society*, vol. 155, no. 2, pp. A164–A171, 2008.

[15] M. Torchio, L. Magni, R. B. Gopaluni, R. D. Braatz, and D. M. Raimondo, "Lionsimba: A matlab framework based on a finite volume model suitable for li-ion battery design, simulation, and control," *Journal of The Electrochemical Society*, vol. 163, no. 7, pp. A1192–A1205, 2016.

[16] G. L. Plett, "Extended kalman filtering for battery management systems of lipb-based hev battery packs: Part 3. state and parameter estimation," *Journal of Power sources*, vol. 134, no. 2, pp. 277–292, 2004.

[17] R. Klein, N. A. Chaturvedi, J. Christensen, J. Ahmed, R. Findeisen, and A. Kojic, "Electrochemical model based observer design for a lithium-ion battery," *IEEE Transactions on Control Systems Technology*, vol. 21, no. 2, pp. 289–301, March 2013.

[18] I.-S. Kim, "The novel state of charge estimation method for lithium battery using sliding mode observer," *Journal of Power Sources*, vol. 163, no. 1, pp. 584–590, 2006.

[19] ——, "A technique for estimating the state of health of lithium batteries through a dual-sliding-mode observer," *IEEE Transactions on Power Electronics*, vol. 25, no. 4, pp. 1013–1022, 2010.

[20] F. Magnusson and J. Åkesson, "Collocation methods for optimization in a modelica environment," in *Proceedings of the 9th International MODELICA Conference; September 3-5; 2012; Munich; Germany*, no. 076. Linköping University Electronic Press, 2012, pp. 649–658.

[21] A. Wächter and L. Biegler, "On the implementation of a primal-dual interior point filter line search algorithm for large-scale nonlinear programming," *Mathematical Programming*, vol. 106, pp. 25–57, 2006.

[22] J. Andersson, J. Åkesson, and M. Diehl, "Casadi: A symbolic package for automatic differentiation and optimal control," in *Recent Advances in Algorithmic Differentiation*. Springer, 2012, pp. 297–307.

[23] N. A. Chaturvedi, R. Klein, J. Christensen, J. Ahmed, and A. Kojic, "Algorithms for advanced battery-management systems," *IEEE Control Systems*, vol. 30, no. 3, pp. 49–68, 2010.

[24] R. D. Perkins, A. V. Randall, X. Zhang, and G. L. Plett, "Controls oriented reduced order modeling of lithium deposition on overcharge," *Journal of Power Sources*, vol. 209, pp. 318–325, 2012.

[25] P. Arora, M. Doyle, and R. E. White, "Mathematical modeling of the lithium deposition overcharge reaction in lithium-ion batteries using carbon-based negative electrodes," *Journal of The Electrochemical Society*, vol. 146, no. 10, pp. 3543–3553, 1999.